Electronic Supplementary Material (ESI) for Journal of Materials Chemistry C.

ELECTRONIC SUPPORTING INFORMATION

A Multifunctional Binder Capable of Harvesting Light, Electronic Transport, and Photocharging a Lithium-Ion Photobattery

Elsa Briqueleur[a], Mickael Dollé[a*] and W. G. Skene[b*]

Tables of Contents

Synthesis of **p(PDI-EO)**……..…….……..3
Table S1. ^{13}C-NMR peak assignment. 3
Table S2. ^{1}H-NMR peak assignment. 4
Table S3. FT-IR frequency assignment of **p(PDI-EO)**. 5
Table S4. Composition of the electrodes presented in Figure 4. 9
Table S5. Assignment of FT-IR frequencies of pristine **p(PDI-EO)**/LFP electrode.[a,S7,S8,S9,S10,S11,S12] 10
Table S6. Assignment of FT-IR frequencies of **p(PDI-EO)**/LFP electrode after 100 hours of OCV in the dark.[a,b] 11
Table S7. Assignment of FT-IR frequencies of **p(PDI-EO)**/LFP electrode after a D/20 discharge followed by 35 hours OCV in the dark.[a,b] 11
Table S8. Assignment of FT-IR frequencies of **p(PDI-EO)**/LFP electrode after a D/20 discharge followed by OCV during illumination (Figure 4).[a,b] 12

Figure S1. Structure and numbering of **p(PDI-EO)** corresponding to Table S1 (m+p=6). 4
Figure S2. Structure and numbering of **p(PDI-EO)** corresponding to Table S2 (m+p=6). 5
Figure S3. GPC elugram of the mass fraction **p(PDI-EO)**, w(log M), in chlorobenzene relative to polystyrene standards in a dM interval. 6
Figure S4. Thermal gravimetric analysis of **p(PDI-EO)** (red line) and Jeffamine® ED-600 (blue line). 6
Figure S5. Scattering (435-485 nm) and emission (485-850 nm) spectra of the **p(PDI-EO)** in dichloromethane (A) and as a thin film drop cast on PET-ITO (B) measured with an integrating sphere relative to a blank substrate (black line). A neutral density filter was used for the solid-state scattering measurements. 7
Figure S6. Solid-state excitation (blue) and emission (black) spectra of **p(PDI-EO)** (solid line) and PDI (dashed line). 7
Figure S7.) Absorbance (A) and emission (B) spectra of **p(PDI-EO)** (solid line) and PDI (dashed line) in dichloromethane. 8
Figure S8. Cyclic voltammogram of **p(PDI-EO)** measured in EC:DMC (1:1) with $LiPF_6$ (1 M) at 0.1 mV/s scan speed in the 2-4 V windows relative to Li^+/Li reference. 8
Figure S9. Ultraviolet photoemission spectrum of **p(PDI-EO)** for determining its valence band (VBM) and work function (WF). 9
Figure S10. SEM micrograph cross-section of **p(PDI-EO)** photoelectrode at 4k magnification. ..9
Figure S11. Fluorescence micrographs of the **p(PDI-EO)** photoelectrode prepared with a polymer:carbon filler:LFP composition of 82:2:16 wt%: top-view magnified 50k (left) and cross-section magnified 20k (right). 10
Figure S12. Schematic representation of the expected light induced imide lithiation by cLFP. 12

Synthesis of p(PDI-EO)

The synthesis of the polymer was adapted from known methods.[1] The modified procedure consisted of 3,4,9,10-perylenetetracarboxylic dianhydride (PTCDA; 800 mg, 2 mmol), Jeffamine® ED-600 (1.23 g, 2 mmol), imidazole (5.0 g, 74.5 mmol) and zinc acetate (385 mg, 2 mmol) that were combined and heated with stirring at 140 °C for 5 h. The temperature was then lowered to 70 °C and hydrochloric acid (1 N, 50 mL) was added to the hot mixture. The mixture was stirred and the temperature was allowed to gradually cool to ambient temperature. The resulting precipitate was collected via vacuum filtration and it was washed with a boiling solution of saturated potassium carbonate followed by boiling distilled water until the pH of the filtrate was neutral. The black solid that was obtained was dried in air at 100 °C before removing the undesired oligomers by washing several times with DMSO. M_n = 17 240 g/mol calculated from $\frac{\Sigma[(mass\ fraction\ by\ dM\ interval) * molecular\ weight]}{\Sigma[mass\ fraction\ by\ dM\ interval]}$; Đ=1.30. Conversion 97% according to the Carothers' equation calculated from the GPC M_n data.

^{13}C-NMR spectroscopy of p(PDI-EO)[S1,S2]

The ^{13}C-NMR (100 MHz) spectrum of p(PDI-EO) was acquired in $CDCl_3$ (40 mg/mL; Table S1). The spectrum was benchmarked against the corresponding constitutional components: PDI ($CDCl_3$ 25 mg/L) and Jeffamine® ED-600 (D_2O). The peaks corresponding to the perylene diimide repeating unit were located after 100 ppm. The polymerization was confirmed by the absence of the characteristic peaks of the anhydride monomer in the 200 ppm region. The Jeffamine® ED-600 repeating unit was assigned to the region below 100 ppm as per Table S1. ^{13}C-NMR ($CDCl_3$, 100 MHz) δ= 163.36, 133.49, 130.70, 123.18, 122.62, 121.54, 75.02, 72.24, 70.50, 48.66, 17.34, 15.26 ppm.

Table S1. ^{13}C-NMR peak assignment.

Chemical shift (ppm)	Assignment
163.36	N-C^{ζ}=O
133.49, 130.70, 123.18, 122.62, 121.54	**Perylene core**
75.02, 72.24, 70.50	C^{δ}-O
48.66	C^{γ}-N
17.34	H3C^{β}-C-O
15.26	H3C^{α}-C-N

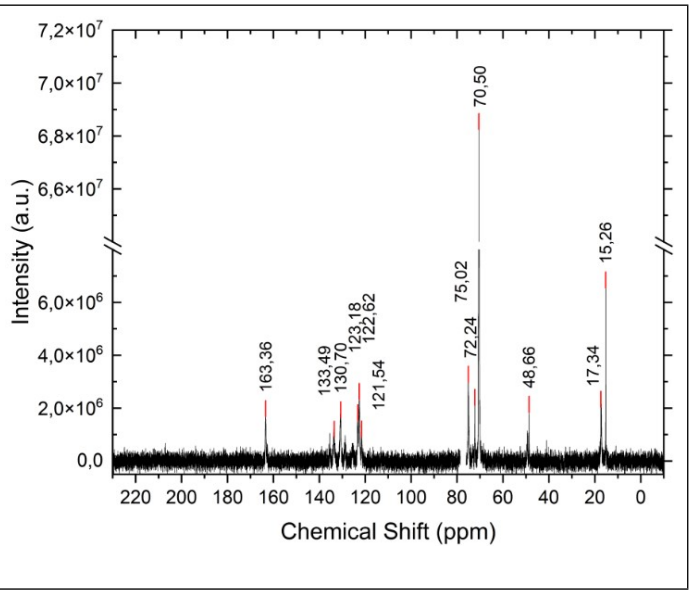

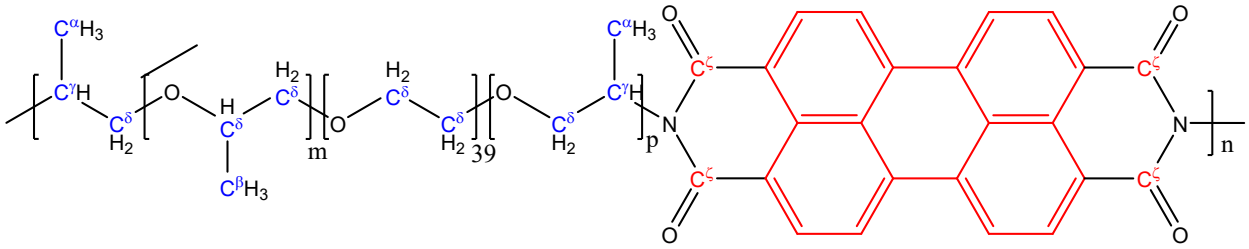

Figure S1. Structure and numbering of **p(PDI-EO)** corresponding to Table S1 (m+p=6).

^{1}H-NMR of p(PDI-EO)

The ^{1}H-NMR (400 MHz) spectrum of **p(PDI-EO)** was measured in $CDCl_3$ (10 mg/mL; Table S2). δ= 8.36, 5.52, 4.27, 3.98, 3.90, 3.67, 2.60, 1.66, 1.28, 1.12 ppm. The unmarked peak remains from the hidden $CDCl_3$ peak (7.28 ppm).

Table S2. ^{1}H-NMR peak assignment.

Chemical shift (ppm)	**Assignment**
8.36	H^{κ}-Ar
5.52	$H2^{\iota}$C-O
4.27	$H2^{\theta}$C-O
3.98	H^{η}C-O
3.90	$H2^{\zeta}$C-O
3.67	$H2^{\varepsilon}$C-O
2.60	$H2^{\delta}$C-N
1.66	$H3^{\gamma}$C-CO
1.28	$H3^{\beta}$C-CN
1.12	$H3^{\alpha}$C-CN

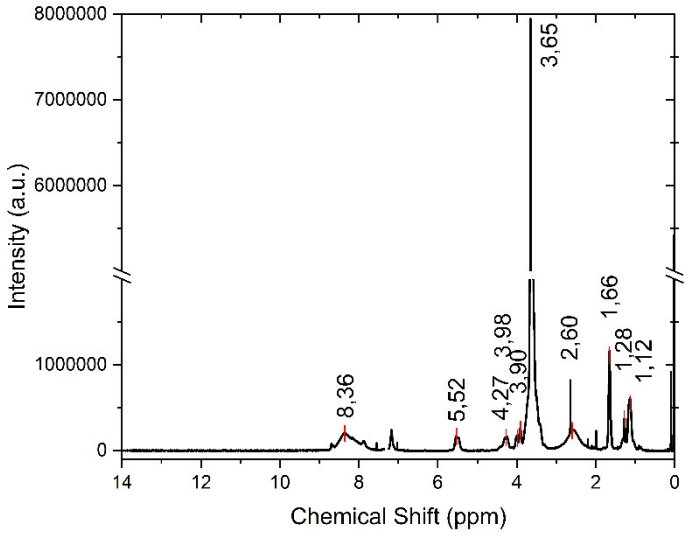

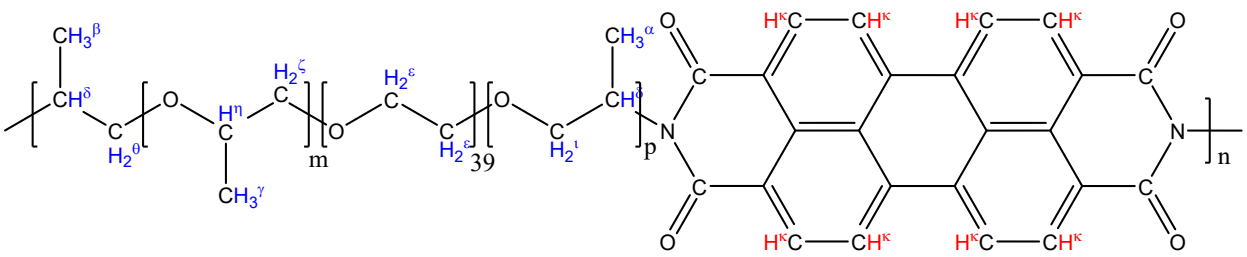

Figure S2. Structure and numbering of **p(PDI-EO)** corresponding to Table S2 (m+p=6).

FT-IR spectroscopy of p(PDI-EO)[S2,S3,S4,S5,S6]

FT-IR spectra of the as-synthesized polymer was measured with an ATR accessory. The vibrations of the copolymer were assigned as per Table S3. No characteristic vibrations in the 1750-1800 cm^{-1} region, corresponding to the carbonyl of the anhydride, were observed and no free amine was found in the 3200-3350 cm^{-1} range. The absence of these characteristic vibrations proves the complete conversion of both the PTCDA and Jeffamine®, respectively, to the title polymer.[S2,S6]

Table S3. FT-IR frequency assignment of **p(PDI-EO)**.

Frequency (cm^{-1})	**Assignment**
2913, 2842	**H-C-H** asym. And sym. Stretching
1697, 1650	**C=O** stretching (imide)
1591, 1501	**C=C** stretching (aromatic)
1464	**H-C-H** bending
1402	**C-C** stretching
1340	**C-N** stretching
1300, 1256	**C-C** stretching
1089	**C-O-C** stretching (ether)
977, 933, 853, 809	**=C-H** bending

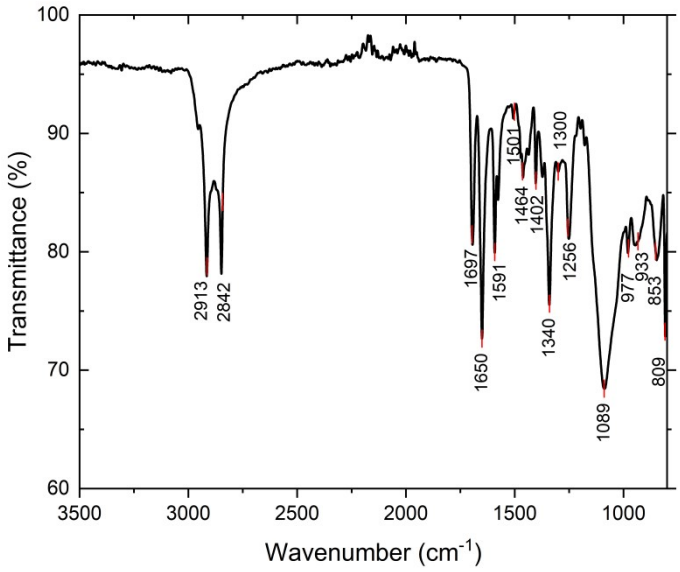

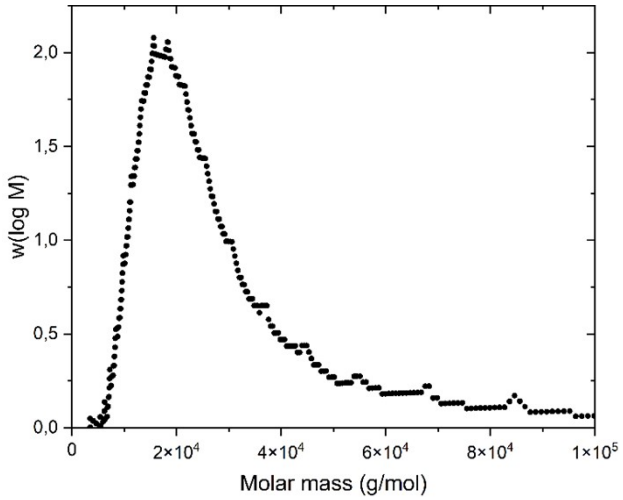

Figure S3. GPC elugram of the mass fraction **p(PDI-EO)**, w(log M), in chlorobenzene relative to polystyrene standards in a dM interval.

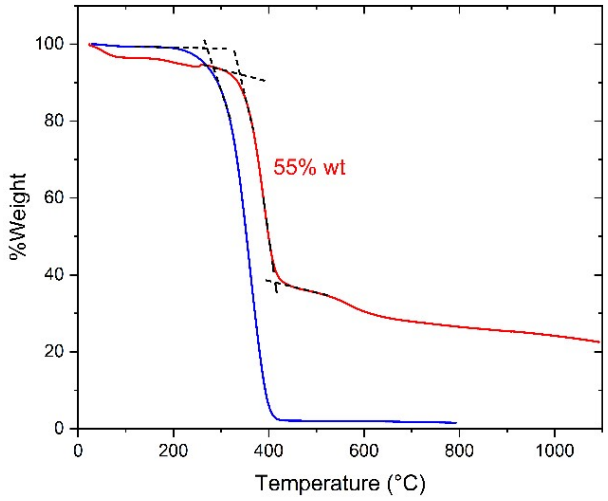

Figure S4. Thermal gravimetric analysis of **p(PDI-EO)** (red line) and Jeffamine® ED-600 (blue line).

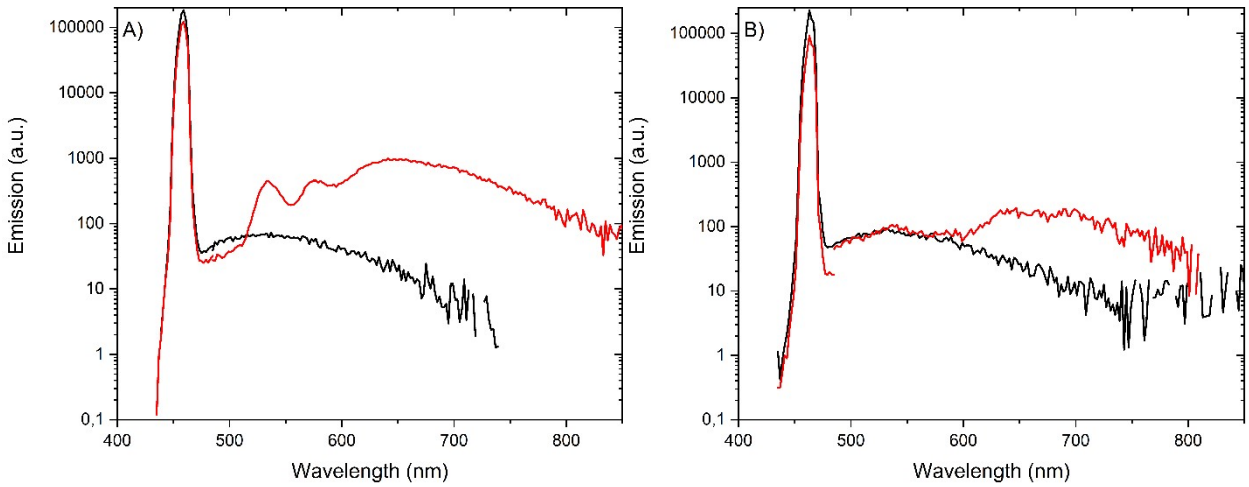

Figure S5. Scattering (435-485 nm) and emission (485-850 nm) spectra of the **p(PDI-EO)** in dichloromethane (A) and as a thin film drop cast on PET-ITO (B) measured with an integrating sphere relative to a blank substrate (black line). A neutral density filter was used for the solid-state scattering measurements.

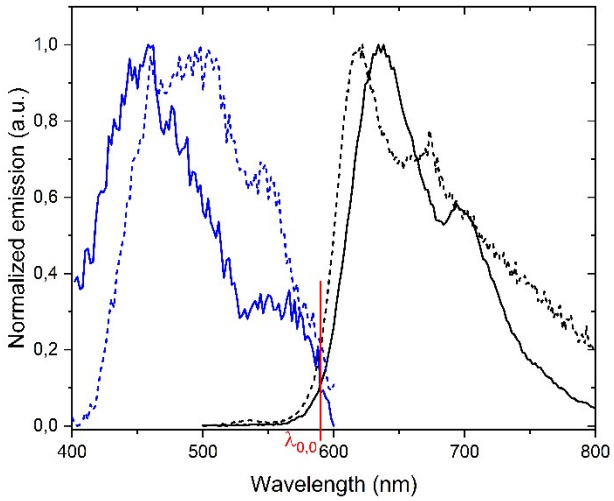

Figure S6. Solid-state excitation (blue) and emission (black) spectra of **p(PDI-EO)** (solid line) and PDI (dashed line). The optical energy gap ($\Delta E_{0,0}$) is calculated from the Planck-Einstein equation from the intersection ($\lambda_{0,0}$) of the normalized absorption and emission spectra at 589 nm (red line).

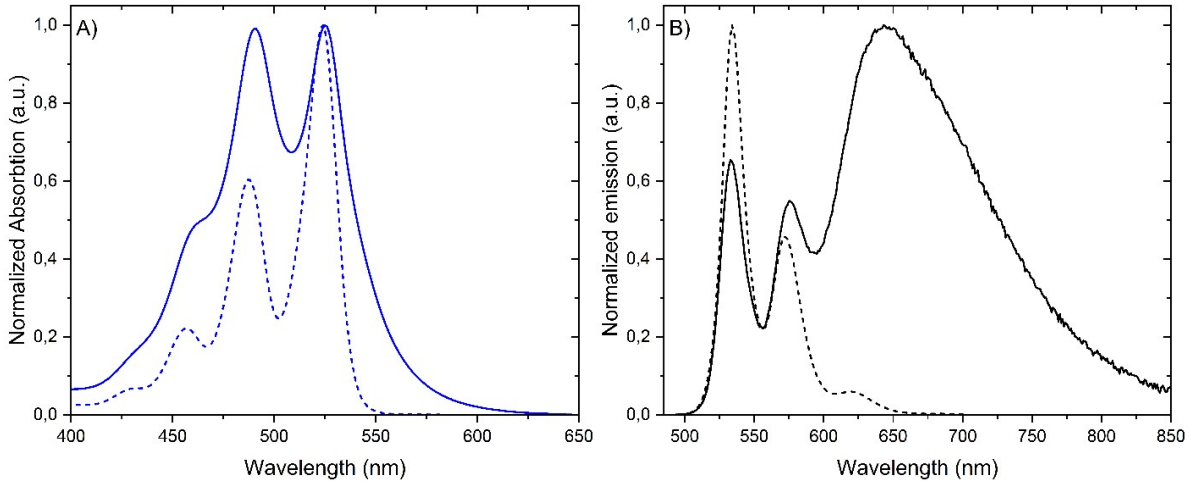

Figure S7. Absorbance (A) and emission (B) spectra of **p(PDI-EO)** (solid line) and PDI (dashed line) in dichloromethane.

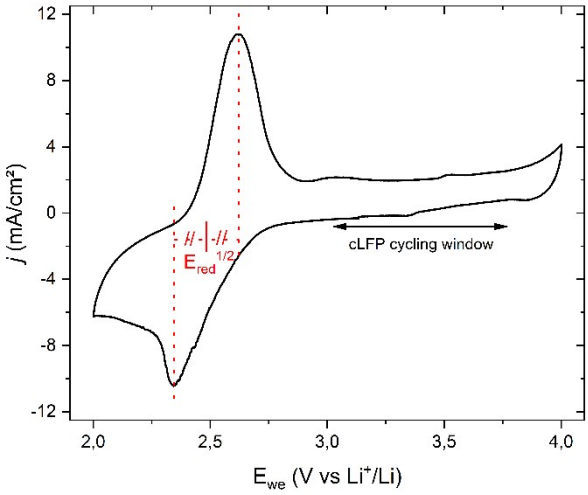

Figure S8. Cyclic voltammogram of **p(PDI-EO)** measured in EC:DMC (1:1) with $LiPF_6$ (1 M) at 0.1 mV/s scan speed in the 2-4 V windows relative to Li^+/Li reference. The black arrow delimits the window for the electrochemical testing. Red dashes correspond to the $E_{red}^{1/2}$=2.47 V vs Li^+/Li.

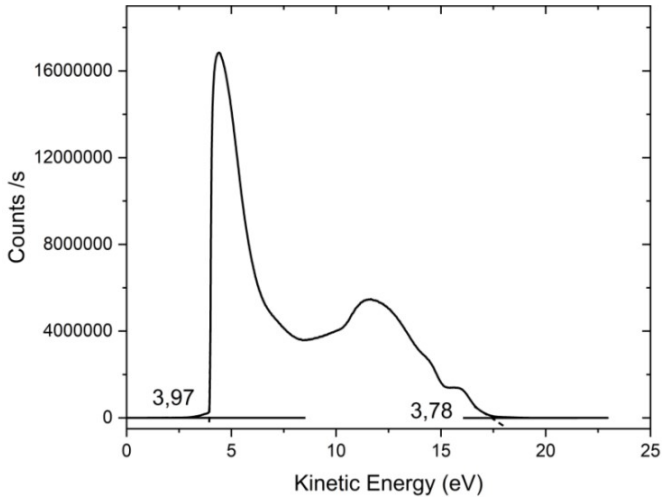

Figure S9. Ultraviolet photoemission spectrum of **p(PDI-EO)** for determining its valence band (VBM) and work function (WF).

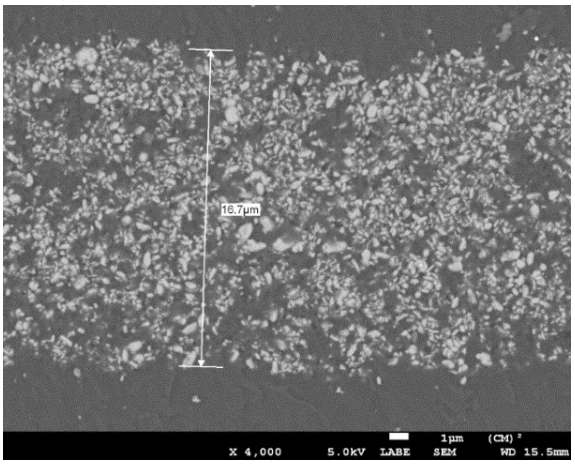

Figure S10. SEM micrograph cross-section of **p(PDI-EO)** photoelectrode at 4k magnification.

Table S4. Composition of the electrodes presented in Figure 4.

Polymer Binder	Electrode composition (cLFP:C65:Binder)	cLFP Loading (mg/cm²)
p(PDI-EO)	(82:2:16)	0.38
PEO 1 000 kg/mol	(82:9:9)	4.79
PEO 1 000 kg/mol	(82:2:16)	3.26
PEO 35 kg/mol	(82:9:9)	2.39
PEO 35 kg/mol	(82:2:16)	3.91

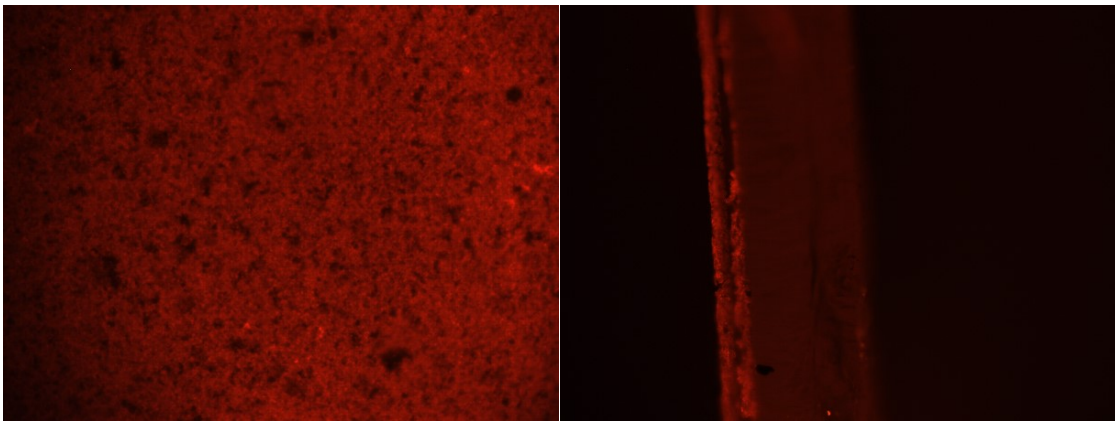

Figure S11. Fluorescence micrographs of the **p(PDI-EO)** photoelectrode prepared with a polymer:carbon filler:LFP composition of 82:2:16 wt%: top-view magnified 50k (left) and cross-section magnified 20k (right).

Table S5. Assignment of FT-IR frequencies of pristine **p(PDI-EO)**/LFP electrode.[a,S7,S8,S9,S10,S11,S12]

Frequency (cm^{-1})	**Assignment**
461, 494, 546, 573	PO_4^{3-} bending
936, 1036, 1136	PO_4^{3-} streching
631, 646	FeO_6
742, 807	=C-H bending
1254, 1403	C-C stretching
1343	C-N stretching
1576, 1591	C=C stretching
1652, 1696	imide C=O stretching

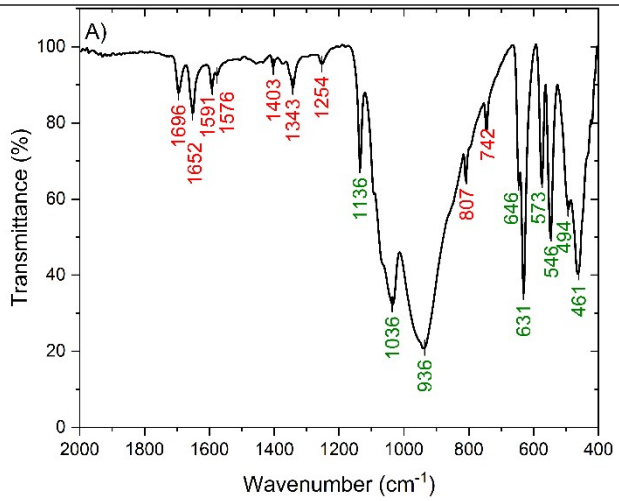

[a] Red=**p(PDI-EO)** and green=cLFP.

Table S6. Assignment of FT-IR frequencies of **p(PDI-EO)**/LFP electrode after 100 hours of OCV in the dark.[a,b]

Frequency (cm^{-1})	**Assignment**
770	S-N and C-S streching, S-N streching, CF_3 bending
797	S-N and C-S streching CF_3 streching
1193	C-F_3 stretching
1345	SO_2 streching
1639	=C-O$^-$Li$^+$ (lithium enolate)

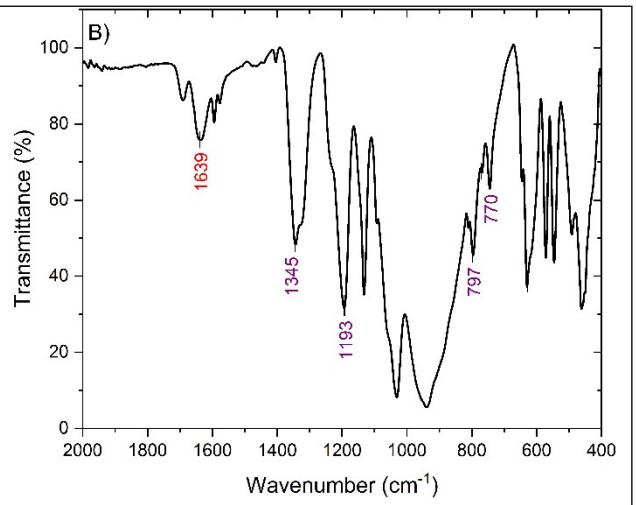

[a] LiTFSI electrolyte in water (3.5 mL, 1 m), $FePO_4$ counter electrode, and Ag/AgCl reference electrode. [b] Only the peaks shifted from Table S5 are assigned. Red=**p(PDI-EO)**; purple=LiTFSI.

Table S7. Assignment of FT-IR frequencies of **p(PDI-EO)**/LFP electrode after a D/20 discharge followed by 35 hours OCV in the dark.[a,b]

Frequency (cm^{-1})	**Assignment**
952	PO_4^{3-} stretching

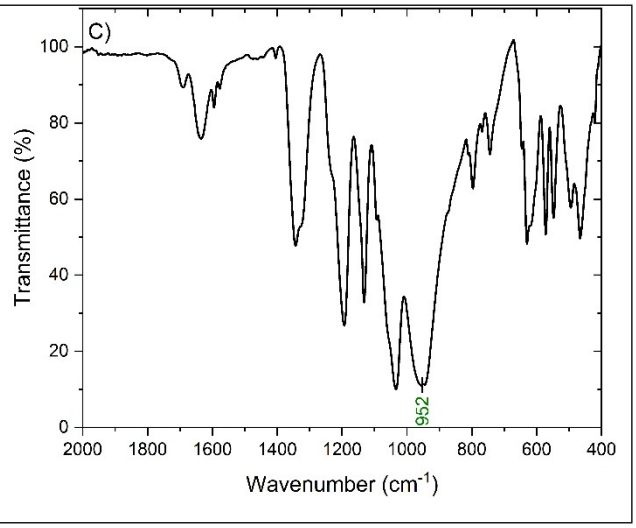

[a] LiTFSI electrolyte in water (3.5 mL, 1 m), $FePO_4$ counter electrode, and Ag/AgCl reference electrode. [b] Only the peaks shifted from Table S6 are assigned. Green=cLFP.

Table S8. Assignment of FT-IR frequencies of **p(PDI-EO)**/LFP electrode after a D/20 discharge followed by OCV during illumination (Figure 4).[a,b]

Frequency (cm^{-1})	**Assignment**
461-506	PO_4^{3-} stretching
548-570	
615	
987-1045	
1581, 1594	C=C stretching
1634	=C-O$^-$Li$^+$ (lithium enolate)
1696	imide C=O stretching

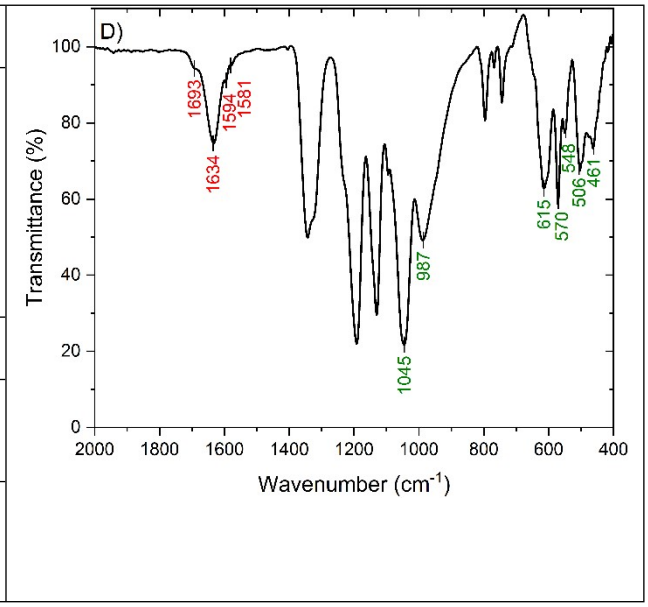

[a] LiTFSI electrolyte in water (3.5 mL, 1 m), $FePO_4$ counter electrode, and Ag/AgCl reference electrode. [b] Only the peaks shifted from Table S7 are assigned. Red=**p(PDI-EO)**; green=cLFP.

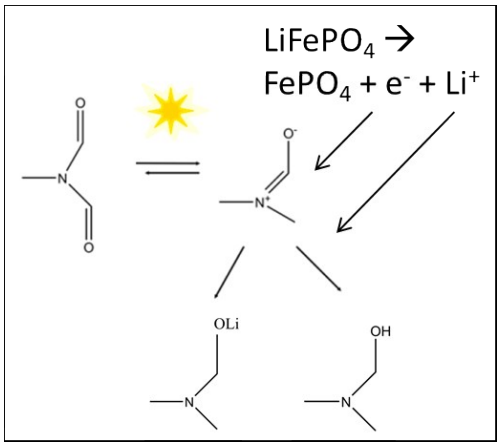

Figure S12. Schematic representation of the expected light induced imide lithiation by cLFP.

References

S1. Sharma, P.; Damien, D.; Nagarajan, K.; Shaijumon, M. M.; Hariharan, M., Perylene-polyimide-based organic electrode materials for rechargeable lithium batteries. *J. Phys. Chem. Lett.* **2013,** *4* (19), 3192-3197.

S2. Aivali, S.; Anastasopoulos, C.; Andreopoulou, A. K.; Pipertzis, A.; Floudas, G.; Kallitsis, J. K., A "Rigid-flexible" approach for processable perylene diimide-based polymers: Influence of the specific architecture on the morphological, dielectric, optical, and electronic properties. *J. Phys. Chem. B.* **2020,** *124* (24), 5079-5090.

S3. Bodapati, J. B.; Icil, H., Highly soluble perylene diimide and oligomeric diimide dyes combining perylene and hexa(ethylene glycol) units: Synthesis, characterization, optical and electrochemical properties. *Dyes Pigm.* **2008,** *79* (3), 224-235.

S4. Glosz, K.; Ledwon, P.; Motyka, R.; Stolarczyk, A.; Gusev, I.; Blacha-Grzechnik, A.; Waskiewicz, S.; Kaluzynski, P.; Lapkowski, M., Functionalized polysiloxanes with perylene diimides and poly(ethylene glycol): Synthesis and properties. *Eur. Polym. J.* **2022,** *162*.

S5. Li, S.; Jiang, X.; Yang, Q.; Shao, L., Effects of amino functionalized polyhedral oligomeric silsesquioxanes on cross-linked poly(ethylene oxide) membranes for highly-efficient CO_2 separation. *Chem. Eng. Res. Des.* **2017,** *122*, 280-288.

S6. Georgiev, N.; Nichev, H.; Petrov, M.; Lovchinov, K.; Dimova-Malinovska, D.; Bojinov, V., Deposition of perylene diimide derivatives for dye-sensitized solar cells. In *Nanoscience Advances in CBRN Agents Detection, Information and Energy Security*, 2015; pp 497-504.

S7. Ait Salah, A.; Jozwiak, P.; Zaghib, K.; Garbarczyk, J.; Gendron, F.; Mauger, A.; Julien, C. M., FTIR features of lithium-iron phosphates as electrode materials for rechargeable lithium batteries. *Spectrochim. Acta A Mol. Biomol. Spectrosc.* **2006,** *65* (5), 1007-13.

S8. Narita, A.; Shibayama, W.; Ohno, H., Structural factors to improve physico-chemical properties of zwitterions as ion conductive matrices. *J. Mater. Chem.* **2006,** *16* (15).

S9. Dong, C.; Xu, F.; Chen, L.; Chen, Z.; Cao, Y., Design strategies for high-voltage aqueous batteries. *Small Structures* **2021,** *2* (7).

S10. Lahiri, A.; Borisenko, N.; Borodin, A.; Olschewski, M.; Endres, F., Characterisation of the solid electrolyte interface during lithiation/delithiation of germanium in an ionic liquid. *Phys. Chem. Chem. Phys.* **2016,** *18* (7), 5630-7.

S11. Kam, W.; Liew, C.-W.; Lim, J. Y.; Ramesh, S., Electrical, structural, and thermal studies of antimony trioxide-doped poly(acrylic acid)-based composite polymer electrolytes. *Ionics* **2013,** *20* (5), 665-674.

S12. Sa'adun, N. N.; Subramaniam, R.; Kasi, R., Development and characterization of poly(1-vinylpyrrolidone-co-vinyl acetate) copolymer based polymer electrolytes. *Sci. World J.* **2014,** 254215.